2018 IEEE/RSJ International Conference on Intelligent Robots and Systems (IROS)
Madrid, Spain, October 1-5, 2018

Soft Curvature and Contact Force Sensors for Deep-Sea Grasping via Soft Optical Waveguides

Clark B. Teeple, Kaitlyn P. Becker and Robert J. Wood[1]

Abstract— **In this work, we show that sensors based on soft, intentionally-lossy optical waveguides are well-suited for soft robotic grasping applications in the deep-sea. Each finger of a soft robotic hand is outfitted with a 2×1 array of optical sensing elements to enable proprioception and contact force sensing. Curvature sensing elements are integrated directly into the structure of a finger, while contact force sensors are fabricated as standalone units and attached afterward. Along with considerations for interfacing with deep-sea remotely operated vehicles (ROVs), models for the effect of bending on light loss and the effect of normal force on strain were used to inform sensor design decisions. Our sensors show sensitivity to curvature over a range of diameters from 8 mm to 76 mm, and sub-Newton force sensitivity. Additionally, sensors were characterized in simulated deep-sea environments at temperatures from -10°C to 50°C and hydrostatic pressures up to 4000 psi. The sensitivity of our curvature sensors is invariant to the temperatures and pressure ranges tested, though contact force sensors decreased in sensitivity as temperatures decreased. Finally, we successfully demonstrate that sensors onboard soft finger actuators can provide informative state feedback during grasping operations in air and water.**

I. INTRODUCTION

Gentle grasping has become particularly relevant for recovering samples of deep-sea organisms. Minimizing damage to organisms while taking samples is critical for biologists to accurately study morphology and DNA expression. Thus, in a recent effort toward gentle deep sea sampling, soft robotic grippers have been used as tools on deep-sea remotely operated vehicles (ROVs) to cause less damage to animals than traditional rigid grippers [1].

Soft robots have been shown to interact more-gently with objects in their environments using minimal control effort compared to rigid robots [2]. However, while compliance allows soft robots to passively adapt their shape to complex or uncertain objects, compliance also introduces uncertainty in the robot's position and applied forces. Uncertainties in actuator positioning, contact force direction, and gripping force make the grasp quality difficult to predict [3], [4]. These uncertainties are magnified when soft robots are teleoperated on ROVs due to limited state feedback provided to the operator.

While gentle deep-sea grasping has been demonstrated, sampling tasks are often still cumbersome and lengthy due to poor estimation of arm, hand, and soft finger positioning. To enhance the robustness of grasping operations to actuator and environmental uncertainty, many studies of under-actuated rigid hands have used on-board proprioception and contact force sensing in gripper control strategies [5], [6], [7]. Using these two pieces of sensor information in the control of soft actuators, we can improve the robustness of grasps and enable quicker, more effective sampling of deep-sea organisms.

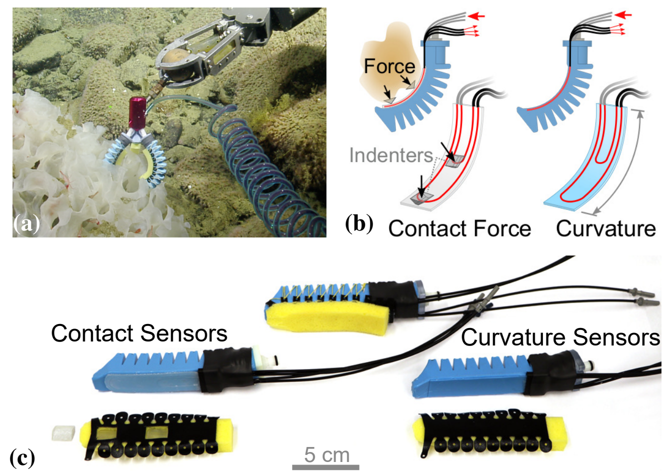

Fig. 1. We outfitted a soft robotic gripper platform developed in our lab with curvature and contact sensors. (a) This platform has been used on a variety of deep-sea sampling expeditions to grasp delicate corals and other organisms. (b) In this work, we use soft optical waveguides as sensors. (c) These sensors are implemented onboard the fingers of the gripper, with curvature sensors integrated directly into the structure.

To implement shape and contact force sensing on soft robots operating in the deep-sea, we chose to use soft optical waveguides. Intentionally lossy, soft waveguides have been used as strain sensing elements in other works through gold-plated elastomer channels [8], and urethane rubber cores surrounded by a silicone cladding [9]. Sensing is accomplished by emitting light into the guide, then measuring the intensity loss of transmitted light as a result of stretching, compressing, or bending.

Compared to other soft sensing modalities, lossy optical waveguides made of elastomers are the most robust for use in the deep-sea, where temperatures reach as low as 2°C and hydrostatic pressures as high as 9000 psi at the ocean floor. The low coefficient of thermal expansion and incompressibility of elastomers makes them insensitive to changes in temperature and hydrostatic pressure. Furthermore, optical properties of elastomers such as refractive index change very little with temperature. Finally, while optical couplings add

*This work was supported by the Wyss Institute for Biologically-Inspired Engineering and the National Science Foundation.

[1]All authors are with the John A. Paulson School of Engineering and Applied Sciences, Harvard University, 60 Oxford St. Cambridge MA 02138, USA cbteeple@g.harvard.edu, kbecker@g.harvard.edu, rjwood@seas.harvard.edu

some complexity, the sensors can be fabricated without local electrical parts to dramatically simplify the waterproofing process necessary for the deep-sea.

By contrast, electrical soft sensors used in soft robots, including resistive and capacitive sensors, are less-suitable for use in the deep-sea. Resistive sensors rely on changes in resistance via deformation of channels filled with conductive liquids (such as liquid metal or ionic liquids), piezoresistive materials, or conductive textiles [10], [11], [12]. These sensors are simple in design, but suffer from thermal drift [13]. In addition, liquid resistive materials such as eGaIn or ionic liquids freeze below $10-18\,^{\circ}$C, rendering them unusable in the deep-sea. Capacitive sensors are usually implemented with similar materials as resistive sensors [14], [15], and tend to be more stable in response to temperature changes, but can be quite sensitive to electrical noise [13].

II. SENSOR DESIGN

A. Design Criteria

In addition to the necessity for invariance to environmental changes mentioned above, a primary objective for our soft sensing elements is the ability to distinguish between bending and external contact forces. This distinction can be made by mechanically decoupling the sensitivity of sensing elements to different modes of deformation through geometry and material selection.

B. Waveguide Design for Soft Fingers

Taking the above criteria into account, we designed the structure of our soft waveguide sensors to enable simple integration with our existing deep-sea soft gripper platform. Waveguides were designed to fit into the 2.5 mm-thick skin of the fingers (bellows-style bending actuators) at the inside of the bend, as shown in Figure 1. The waveguides are patterned in loops that begin and end on the proximal side of the finger for ease of optical connections. The smallest reliable waveguide diameter was 1 mm due to fabrication limitations (discussed later), so only two waveguides could be placed into the volume of the flat face of each finger. Further fabrication refinement may enable the incorporation of more waveguides.

To achieve total internal reflection in our waveguides, the core material for both sensors is ClearFlex 30 (Smooth-On Inc.). Clear-Flex was chosen for its high refractive index of 1.488 to maximize the difference between the indices of the core and silicone cladding (approximately 1.38-1.41). This material combination promotes total internal reflection for angles of incidence up to approximately 18° - 22°.

Materials for the sensor body (which also acts as the optical cladding) are chosen using mechanical stiffness matching [16] by taking into account the stiffnesses of actuators and target objects to be grasped. To design a bending sensor that is relatively insensitive to contact forces, we seek to maximize the cladding material stiffness while being limited by the stiffness of an actuator. Thus, it is convenient to use the same material as the finger actuators, Smooth-Sil 950 (Smooth-On Inc.). To design a maximally sensitive contact

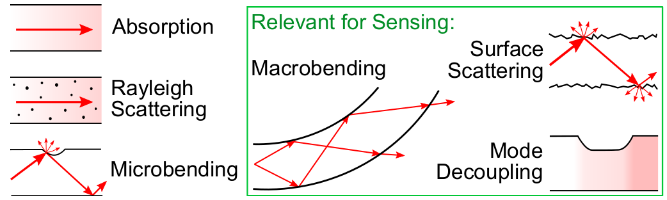

Fig. 2. Large optical waveguides have several important loss mechanisms, some of which can be ignored when modeling intensity loss in our sensors. Absorption, volume scattering, and microbending will be ignored because they remain roughly constant regardless of deformation.

force sensor, we used Ecoflex 00-30 (Smooth-On Inc.) as the cladding material because of its extremely low stiffness (27 times smaller elastic modulus than Smooth-Sil 950). Practically, Ecoflex 00-30 is also the lowest-stiffness silicone we can use before our fabrication method fails.

Finally, we amplify the effect of distributed contact force on the finger by including rigid indenters attached across each waveguide. These indenters amplify contact pressure from objects directly onto the fibers, as shown in Fig. 1.

C. Deep-Sea Interface Design

We used commercially available plastic optical fiber in a modular design to allow the soft sensing elements to interface with typical ROV systems. The plastic optical fibers transmit light between the soft sensing elements and optoelectronics, allowing all electronics to be located proximally in a waterproof and depth-proof container. In addition, modular quick optical disconnects enable easy swapping of actuators and sensors in the field.

III. MODELING OPTICAL LOSSES AS A FUNCTION OF DEFORMATION

To understand how design decisions affect sensor performance, we used simple models for geometric optical losses in our soft optical fibers as well as material deformation and stress. The effect of normal strain on the optical losses in our soft waveguides is much more complex, so the relationship between compression and optical intensity loss is not modeled.

Optical waveguides have several loss mechanisms due to the complexity of light transmission through a waveguide, as shown in Fig. 2, however many of them can be ignored for modeling purposes. We are only interested in the intensity loss incurred as a function of deformation, so we define the intensity loss I_{loss} in decibels as:

$$I_{loss} = 10\log_{10}\left(\frac{I_0}{I}\right) \quad (1)$$

where I is the measured intensity, and I_0 is the baseline intensity under no deformation.

A. Curvature Sensors

To construct a model for curvature losses in our soft optical fibers, we can focus on macrobending and surface roughness as the primary loss mechanisms. The effect of macrobending has been well-studied for circular optical fibers. Our waveguides have substantially rounded corners,

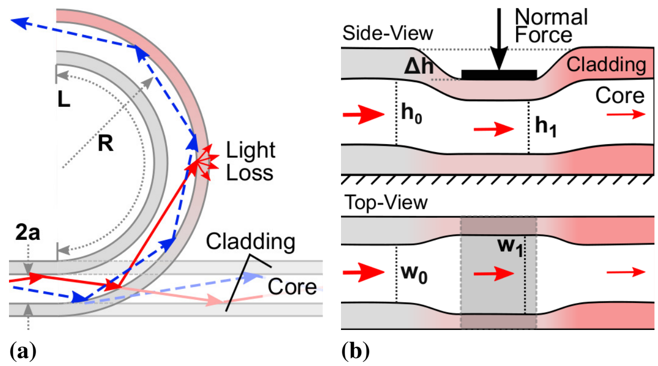

Fig. 3. Schematic diagrams of optical phenomena in soft waveguides during (a) bending and (b) normal force application, including key dimensions and light loss modes.

so we assume an approximately-circular cross-section. As such, the attenuation coefficient, α_B, per unit length in a fiber undergoing a bend with curvature κ can be written as [17]:

$$\alpha_B = C_{b,1} \exp\left(-\frac{n_{core}^2 - n_{clad}^2}{a}\frac{1}{\kappa}\right) \tag{2}$$

where n_{core} and n_{clad} are the refractive indices of the core and cladding, a is the radius of the waveguide, and $C_{b,1}$ is a constant. Using Beer's law, we can find the total power around a bend of length L to be $I = I_0 \exp(\alpha_B L)$. We can rearrange Beer's law into the form in Eq. 1 to obtain the loss per unit length around the bend in dB/cm:

$$I_{loss,mb} = C_{b,2}\alpha_B \tag{3}$$

where $C_{b,2}$ is a constant that transforms the units to decibels and the base of the exponent to base 10.

The role of surface roughness in bending losses has not been studied thoroughly in the literature, but plays a critical role in the bending behavior of soft waveguides in this work and others [9]. The bending response is highly dependent on the direction of curvature due to differences in surface roughness on opposing surfaces of the guide, (a by-product of the fabrication process as discussed in Section IV-A).

We can gain an intuition for how surface roughness affects the relationship between bending and optical intensity loss by examining the simplified problem of a planar waveguide (see Fig. 3a). At rest, light rays propagate with an equal number of reflections on both surfaces of the guide. However, during bending, light begins to reflect more often on the outer surface (dashed blue rays in Fig. 3a). Thus, with a rough outer surface, substantial bending losses occur at much smaller curvatures (larger radii) than pure macrobending. When bent in the opposite direction (smooth outer surface), macrobending takes over (a phenomenon seen in [9] as well).

B. Contact (Normal) Force Sensors

To construct a model for losses in our sensors as a function of input force on a rigid indenter, we need a material model and an optical loss model. In this work, we use the neo-Hookean material model, but only develop an intuition for the optical losses as a function of compression due to the complexity of the problem.

We begin with a cross section of the soft optical sensor with an applied force from a flat indenter, as shown in Fig. 3b. The indenter is displaced into the sensor, which compresses the sensor body (cladding and core), inducing a local change in cross-section of the fiber and a small bend at either edge.

Under uniaxial compression, we relate the axial engineering strain, ε, exhibited in the sensor body to the applied axial engineering stress, σ_{zz}, using the Neo-Hookean material model for large deformations, a common material model for elastomers. This relationship takes the form:

$$\sigma_{zz} = C_1\left(\lambda(\varepsilon) - \frac{1}{\lambda(\varepsilon)^2}\right) \tag{4}$$

where C_1 is a material constant and λ is the principle stretch. Rather than implement this material model for the core and both cladding layers in series, we assume the ratio of core to cladding stiffness is large enough to ignore the effect of cladding compression. Thus, we approximated C_1 based on the Young's modulus and Poisson's ratio of the core (roughly 0.5 MPa and 0.47 respectively).

Based on a high-level analysis, it is likely that the majority of optical intensity losses come from the small bends produced on either side of the indenter, not optical mode de-coupling. Due to the large dimensions of our waveguides (1 mm side lengths), there exist on the order of 10^7 optical transmission modes. A rigorous analysis would require a sum of mode overlap integrals over all modes [18]. However, only the highest-order modes with the lowest power densities would be attenuated due to dimension changes in the waveguide. Thus, mode de-coupling is likely not a major source of losses. The small bends on either side of the indenter are the only remaining loss mechanism, so we would expect the relationship between compressive strain and optical loss to remain roughly similar regardless of indenter size.

IV. METHODS

We designed and fabricated soft waveguide sensor arrays (2×1) both as discrete units and integrated into the structure of our existing soft finger actuators. We then characterized the light loss in these sensors as a function of curvature and local normal force.

A. Fabrication of Soft Waveguides

The fundamental building block in both curvature and contact sensors is a soft waveguide, developed and fabricated using molding methods similar to those presented in [9] and [11]. Waveguides are molded by creating channels in the cladding material, then filling the channels with core material. In the case of discrete sensors, this cladding material is a strip of rubber only slightly thicker than the optical core (as seen in Fig. 4h). When integrated into the structure of a soft finger (as is the case for our curvature sensors), the cladding material is the skin of the flat face of the finger (as seen in Fig. 4b).

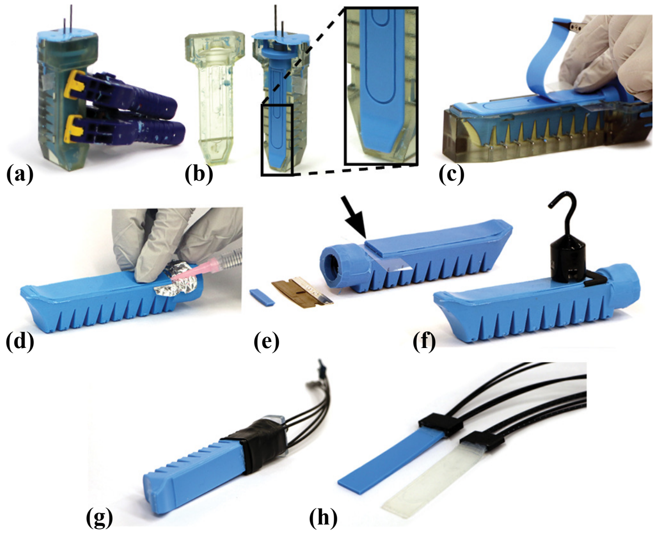

Fig. 4. Fabrication process for soft robotic finger actuators with integrated soft waveguides. (a) The finger actuator is molded per [1], partially cured, then (b) part of the mold is removed exposing channels that create three walls of the waveguide cladding. (c) A separate rubber graft is wet-bonded over the open channels per [11]. (d) Once fully cured, the channels are injected with the core material. (e) Once fully cured, the proximal end is trimmed and (f) glued into an alignment clip. Plastic optical fibers are glued into the other side of the clip. (g) Finger actuator with integrated optical curvature sensor array. (h) Discrete soft optical sensor arrays.

B. Fabrication of Integrated Curvature Sensors

The methods below (and in Figure 4) focus on the fabrication of curvature sensors integrated into the structure of bellows-style soft finger actuators. Due to fabrication limitations, contact sensors are molded as discrete sensors, then adhered to the flat face of actuators. The process modification for discrete units is described later in this section.

To create a finger with integrated waveguides, a mold of our typical bellows-style bending actuator was modified to include grooves (with a square cross-section) that later become waveguides. The mold also accommodates alignment clips for plastic optical fibers that interface with the soft waveguides. The molds were 3D printed on a Stratasys Objet 30 printer with polyjet VeroBlue and VeroClear material, then baked overnight in an oven at 60 °C before use.

Next, the bellows actuator is molded from Smooth-Sil 950 and placed in a pressure chamber according to the procedure described in [1], as shown in Fig. 4a. The actuator is removed from the pressure chamber before it has finished curing (4 hours from silicone mix time), and the channel-side face is removed to expose the flat side of the finger (Fig. 4b). From here, a flat graft of Smooth-Sil 950 is wet-bonded to the exposed flat face of the finger using the procedure found in [11], creating enclosed channels (Fig. 4c). Everything is then cured overnight at room temperature. The resulting roughness on the channel walls formed by the printed mold are much rougher than the grafted side of the channel (atomically smooth) because the new layer of rubber is cured in-place without any surface contact.

After the finger is fully cured, the channels are cut open at the proximal end of the finger, and the core of the optical waveguides is created. Clear-Flex 30 (Smooth-On, Inc.) is degassed and injected into each of the cladding channels until it comes out the other side (Fig. 4d). The assembly is then allowed to cure at room temperature overnight.

With the soft optical waveguides fully formed, rigid plastic optical fibers are aligned and adhered. First the proximal section of the sensor is cut with a razor blade to ensure the a clean optical surface (Fig. 4e). Then, 9-inch lengths of plastic optical fiber (Industrial Fiberoptics, 1 mm core diameter) are aligned with the soft waveguides using a custom-designed 3D printed alignment clip (Markforged, Onyx). The clip is adhered to the finger by silicone adhesive (Silpoxy, Smooth-On), and a strong physical and optical bond between the soft urethane cores and the plastic fibers is made with a cyanoacrylate glue (Loctite 401). Finally, the entire assembly is placed under a 1 kg mass until all adhesives are cured.

To finish the fingers with integrated sensors, the opening to the finger is plumbed with a custom 3D printed adapter and pneumatic hardware, heat shrink tubing is placed around the base of the finger (and alignment clip), and open-cell memory foam is attached to the flat face of the finger. All of these steps follow the procedure described in [1].

To create a discrete 2×1 sensor array, the finger mold is replaced with a flat, rectangular mold to generate three sides of the channel. All subsequent steps (applying the flat graft, cutting the proximal end, attaching plastic optical fibers via alignment clip) remain the same.

C. Fabrication of Contact Force Sensors

To make contact sensors, Ecoflex 00-30 is used as the cladding, while the core remains Clear-Flex 30. Since the cladding material is different from the material used to make the finger, direct integration would pose significant fabrication challenges. Instead, discrete contact sensor arrays are adhered to the flat face of a finger using silicone adhesive (Silpoxy). In addition, 3D printed rigid indenters (Markforged, Onyx) are embedded into the memory foam with the pointed edge directly overtop of the soft waveguides, as seen in Fig. 1c.

D. Data Acquisition and Processing

To acquire light intensity signals from our sensors, red LEDs designed to couple with 1mm fiber (SP000063802, Broadcom Limited) provide a light source, and custom designed acrylic housings allow digital light intensity sensor chips (LTR-329ALS-01, Lite-on Inc.) to couple with the fibers. We used a microcontroller (Arduino Nano, 16 MHz) to interface digitally with the light intensity sensors. Ranges were chosen on a case-by-case basis to maximize the resolution without saturating. All data were captured at 10 Hz, which is more than sufficient for our fingers operating underwater at frequencies much less than 1 Hz.

V. SENSOR CHARACTERIZATION

A. Characterization of Discrete Sensors

Characterization procedures were performed on each type of discrete sensor based on its intended use (curvature and normal force). These calibration procedures are intended to

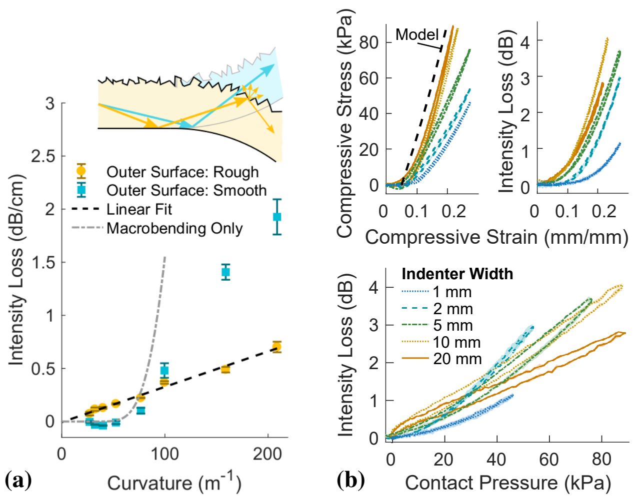

Fig. 5. The sensitivity of discrete curvature and contact force sensors show similar trends to our models and intuition. (a) The intensity loss as function of curvature follows a linear relationship when the outer surface is rough, and agrees in shape with the macrobending model when the outer surface is smooth. (b) Models for stress as a function of strain (upper left) are validated by experimental data, and the intensity loss vs. strain curves (upper right) are roughly invariant to indenter width, validating our intuition. These two relationships combine to form the desired calibration curve (bottom). *Data points in (a) represent the mean of $n = 20$ trials, and curves in (b) represent the mean of $n = 3$ trials.*

approximate field conditions while also isolating the effects of bending and local normal force. While the variation in sensitivity among sensors was not quantified, large variations in the baseline intensity (within approximately 50%) were noted, stemming from variation in soft fiber alignment.

1) Curvature Sensors: The effect of bending on light loss in our sensors was investigated by manually bending standalone sensors around cylinders ranging from 7.9 mm to 76 mm in diameter, as exhibited in the supplementary video. Under typical actuation pressures ($<$ 25 psi), the fingers exhibit curvatures of at most 52 m^{-1} (corresponding to a diameter of 38 mm). For diameters larger than 25 mm, the cylinders were attached to the tip of the sensor body with tape and rolled toward the base. For smaller diameters, the sensors were bent 180 degrees around stationary cylinders.

Calibration curves are based on the intensity loss (as defined in Eq. 1) per unit length around the bend that occurs at the point of maximum bend length for each cylinder. This corresponds to the peak intensity loss during the rolling procedure, producing calibration curves as shown in Fig. 5a.

2) Contact Sensors: The effect of applied normal force on light loss in our sensors was characterized by pressing flat indenters into the sensor using an Instron uniaxial material testing machine. The indenters were 3D printed (Polyjet VeroWhite) with widths ranging from 1 mm to 20 mm, and a length of 20mm, spanning the width of the sensors. The sample (2.2 mm thick) was compressed by 0.6 mm and released at a strain rate of 0.05 mm/sec while recording the resulting axial force and light intensity (see supplementary video).

The calibration curve for force sensors is defined using the contact pressure (force divided by estimated indenter area) vs. intensity loss measurements averaged over three trials for each indenter, as shown in Fig. 5b. It should be noted that contact sensors are also sensitive to curvature due to fabrication limitations, however this effect can be compensated by simultaneously measuring curvature using the curvature sensors.

B. Characterization of On-board Sensors

Curvature and contact sensors implemented on-board each soft finger were characterized in response to finger actuation pressure, curvature, and contact force (if applicable). The effect of actuation pressure on intensity loss was characterized for both types of sensors by blocking the finger's bending motion and applying pressure up to 24 psi in steps of 2 psi. The effect of curvature was characterized for both types of sensors using the same procedure as for standalone curvature sensors without actuating the finger. The effect of contact force on contact sensors was characterized by manually pressing the embedded indenter against a load cell.

The calibration function used to describe intensity loss I_{loss} as a function of actuation pressure p_a, curvature κ, and contact force f_c on a finger is derived from empirical observations:

$$I_{loss} = a_1 \exp(a_2 p_a) + a_3 \kappa + a_4 f_c \tag{5}$$

where a_i are calibration constants. For each finger, parameters a_1 and a_2 were fit using a nonlinear least squares regression on data from blocked actuation tests. a_3 and a_4 were characterized using the datasets from curvature and contact tests respectively.

VI. EVALUATION OF MODELS AND EXPERIMENTS

Experimental characterization of discrete curvature and contact sensors show similar trends to our models, as shown in Fig. 5. The curvature response of the curvature sensors agree in shape with pure macrobending when the outer surface of the bend is smooth, but show a strong linear relationship when the outer surface is rough. In addition, the relationship between compressive strain and stress in contact sensors agrees with the Neo-Hookean model. Finally, The optical loss as a function of compressive strain appears to be loosely invariant to indenter width for indenters wider than 1 mm, confirming our intuition that the majority of light loss is likely due to the small bends on the edges of the indenters.

We can use trends predicted by our models to estimate how changes in design parameters might affect sensor performance. For example, to increase the linearity of curvature the sensors, we should decrease the effects of macrobending and increase the effects of surface roughness. The macrobending model suggests a dependence of $\exp(-a^{-1})$ on the channel size and a dependence of $\exp(-n_{core}^2 - n_{clad}^2)$ on the refractive indices. Thus, we might consider decreasing the channel size a, or increasing the difference in refractive index between the core and cladding to lower the losses from macrobending. We could also consider introducing small surface roughness to linearize the response. Similarly, the force model suggests

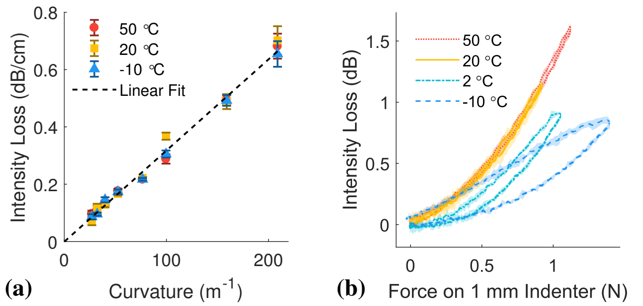

Fig. 6. The bending sensitivity of our soft fiber-optic sensors is invariant to operating temperature, while normal force sensitivity decreases with decreasing temperature. (a) Invariance of curvature sensors is illustrated by an overlap in calibration data for all curvatures measured. (b) However, temperature dependence of force sensors is illustrated by calibration tests with a 1 mm flat indenter. *Curvature points represent the mean of $n = 20$ repetitions for a single sensor. Force curves represent the mean of $n = 3$ trials. Error bars/regions represent one standard deviation from the mean.*

a direct dependence on the material parameter C_1 in eqn. 4 which is proportional to elastic modulus, and inversely dependent on area. Therefore, to increase sensitivity to applied force, we could minimize the elastic modulus or the area of the indenter.

VII. CHARACTERIZATION UNDER DEEP-SEA CONDITIONS

To determine the extent to which our soft optical sensors are affected by deep-sea conditions, we tested performance under simulated environments. Operating temperature and hydrostatic pressure effects were explored separately.

A. *Temperature*

The effect of operating temperature was evaluated using discrete curvature sensors and contact sensors at different ambient temperatures. Sensors were equilibrated for 15 minutes on a heating/cooling plate (Teca, Model AHP-301CPV) set to a desired temperature ($-10°$C, $20°$C, or $50°$C). After equilibration, either a curvature or indentation calibration procedure (described in Section V-A) was performed directly on the temperature plate. Comparisons of calibration curves for one curvature and one contact force sensor at temperatures from $-10°$C, to $50°$C are shown in Figure 6.

Based on these temperature-controlled results, we have determined that the bending sensitivity of our soft fiber-optic sensors is invariant to operating temperature within the measured range. This makes sense because our curvature sensors are thin sheets that are sensitive to geometric optical losses, but they only incur small deformation in the material.

However, the normal force sensitivity of our sensors decreases as temperatures drop below room temperature. This makes sense because optical properties of materials do not change very quickly with temperature, but the elastic moduli of elastomers usually increase as temperatures decrease. In addition, the force sensors show a dramatic increase in hysteresis as the temperature drops below $0°$C. This also makes sense due to the viscoelasticity of the polyurethane core material, which could be improved by material choice.

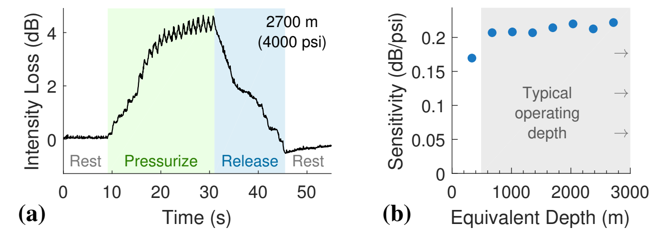

Fig. 7. The sensitivity of integrated curvature sensors does not change appreciably under typical deep-sea hydrostatic pressures. Pressure testing was performed in a pressure vessel at $4°$C with the ability to actuate a finger. (a) Sensor readings are shown from a typical actuation cycle from 0 psi up to 21 psi and back down to 0 psi gauge pressure, with the large steps caused by successive pumps of the hand pump. (b) shows the sensitivity of the integrated curvature sensor as a function of equivalent depth.

Finally, while the quasi-static sensitivity of our sensors exhibit the relationships described, the dynamic characteristics such as bandwidth are likely very temperature-dependent. These effects were not characterized in this work because deep-sea sampling procedures performed *in-situ* are slow enough to assume quasi-static conditions.

B. *Hydrostatic Pressure*

The effect of hydrostatic pressure on the sensitivity of our curvature sensors was characterized using a finger actuator with integrated curvature sensor array as well as a second discrete sensor array. Both were placed into a vessel pressurized between 0 psi and 4000 psi (2700m equivalent depth) with $4°$C tap water using a pump and back-flow valve, as shown in the supplementary video. Optical sensing circuitry was waterproofed and connected to a pressure-rated electrical passthrough so sensor readings could be collected from outside the vessel.

Under high pressure, the finger was actuated and the resulting combined sensitivity to internal pressure and curvature was found. At each increment of high pressure, the finger's internal pressure was first allowed to equilibrate, then a hand pump was used to pressurize the finger to a gauge pressure of 21 psi (set by an internal check valve), then the finger was vented back to the vessel pressure. An example of sensor readings during these actuation cycles is shown in Fig. 7. The sensitivity of the sensor at each pressure was calculated as $S_{pres} = I_{loss,max}/P_{max}$, where $I_{loss,max}$ is the maximum intensity loss over one actuation cycle, and P_{max} is 21 psi.

Based on these tests, the sensitivities of our integrated curvature sensors are reasonably invariant to the combined effects of low temperatures and hydrostatic pressure beyond 1000 psi (700 m equivalent). This implies that curvature calibration done anywhere in this pressure range would be valid for the rest of the pressure range tested.

VIII. GRASPING OBJECTS

To demonstrate how our integrated sensors can provide informative feedback during grasping, we performed grip-pull tests with a rigid cylinder, and underwater grasps of a compliant sphere. In the grip test, two fingers were mounted

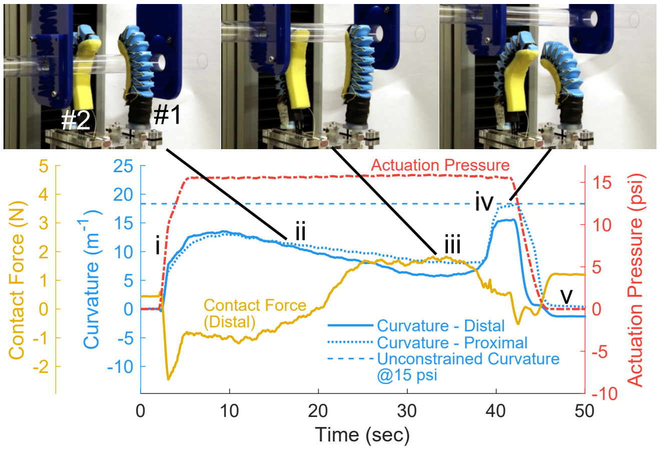

Fig. 8. Grasping a cylinder shows key points where curvature and contact force sensors provide more information than internal pressure alone. At *i*, the fingers are pressurized to 15 psi, but blocked by the cylinder. The cylinder is then moved upward, forcing fingers to straighten (*ii*). The cylinder continues upward until it reaches the fingertips (*iii*) and eventually slips out of the grasp, allowing the fingers to reach their unconstrained curved positions (*iv*). Finally, the fingers are de-pressurized (*v*).

to the base of the Instron: Finger #1 with two integrated curvature sensors, and finger #2 with one functioning contact sensor. The fingers were actuated to grasp a cylinder of 1 in diameter, which was then pulled out of the grasp. The resulting curvature and contact force estimates are shown in 8, where finger #2's contact force estimate is curvature-corrected using the curvature estimates from finger #1. As shown, the curvature estimates provide higher-fidelity information about the grasp than actuation pressure alone. In addition, we performed underwater pick-and-release operations on an extremely compliant sphere to demonstrate successful sensor function underwater, as can be seen in the supplementary video.

IX. CONCLUSIONS

In summary, we have designed and integrated soft optical waveguide sensors on-board the fingers of a soft robotic hand that enable proprioception and contact force measurements. We validated the function of the sensors in deep-sea conditions, and demonstrated their ability to provide useful state feedback during grasping in both air and water.

In future work, the sensitivity of contact sensors should be increased through improved modeling, the density of sensors in each finger should be increased by improving fabrication techniques, and other types of sensors could be explored such as multi-axis contact sensing. Application of these sensors in deep-sea soft manipulators will enable improved sampling of organisms through enhanced state feedback, and can be extended to enable grasp planning and other high-level autonomous behavior.

ACKNOWLEDGMENTS

The authors would like to thank Daniel Hoer and the Girguis Lab at Harvard for helping with pressure testing, Brennan Phillips and Daniel Vogt for discussions about deployment and fabrication, Huichan Zhao for inspiration and helpful discussions, Anna Shneidman for helpful discussions on modeling, David Gruber for his intuition and vision for the future of deep-sea grippers, Moritz Graule for helpful discussions, as well as Ocean Engineering Trust and the Nautilus team.

This work was supported by the Wyss Institute for Biologically Inspired Engineering; the National Science Foundation (under award 1556164); and the National Science Foundation Graduate Research Fellowship (under grants DGE1144152 and DGE1745303). Any opinions, findings, conclusions, or recommendations expressed in this material are those of the authors and do not necessarily reflect those of the funding organizations.

REFERENCES

[1] K. C. Galloway, K. P. Becker, B. Phillips, J. Kirby, S. Licht, D. Tchernov, R. J. Wood, and D. F. Gruber, "Soft Robotic Grippers for Biological Sampling on Deep Reefs," *Soft Robotics*, vol. 3, no. 1, p. soro.2015.0019, 2016.

[2] D. Rus and M. T. Tolley, "Design, fabrication and control of soft robots," *Nature*, vol. 521, no. 7553, pp. 467–475, 2015.

[3] Q. Wan and R. D. Howe, "Modeling the Effects of Contact Sensor Resolution on Grasp Success," *IEEE Robotics and Automation Letters*, vol. 3, no. 3, pp. 1933–1940, 2018.

[4] M. R. Cutkosky and I. Kao, "Computing and Controlling the Compliance of a Robotic Hand," *IEEE Transactions on Robotics and Automation*, vol. 5, no. 2, pp. 151–165, 1989.

[5] L. P. Jentoft, Q. Wan, and R. D. Howe, "Limits to compliance and the role of tactile sensing in grasping," *Proceedings - IEEE International Conference on Robotics and Automation*, pp. 6394–6399, 2014.

[6] Q. Wan, R. P. Adams, and R. D. Howe, "Variability and predictability in tactile sensing during grasping," *IEEE International Conference on Robotics and Automation*, vol. 2016-June, pp. 158–164, 2016.

[7] L. U. Odhner, L. P. Jentoft, M. R. Claffee, N. Corson, Y. Tenzer, R. R. Ma, M. Buehler, R. Kohout, R. D. Howe, and A. M. Dollar, "A compliant, underactuated hand for robust manipulation," *The International Journal of Robotics Research*, 2014.

[8] C. To, T. L. Hellebrekers, and Y.-L. Park, "Highly stretchable optical sensors for pressure, strain, and curvature measurement," in *2015 IEEE/RSJ International Conference on Intelligent Robots and Systems (IROS)*. IEEE, sep 2015.

[9] H. Zhao, K. O'Brien, S. Li, and R. Shepherd, "Optoelectronically Innervated Soft Prosthetic Hand via Stretchable Optical Waveguides," *Science Robotics*, vol. 7529, no. December, pp. 1–10, 2016.

[10] R. K. Kramer, "Soft electronics for soft robotics," in *Micro and Nanotechnology Sensors, Systems, and Applications VII*, T. George, A. K. Dutta, and M. S. Islam, Eds. SPIE-Intl Soc Optical Eng, 2015.

[11] D. Vogt, Y.-L. Park, and R. J. Wood, "A soft multi-axis force sensor," in *2012 IEEE Sensors*. Institute of Electrical and Electronics Engineers (IEEE), oct 2012.

[12] J. C. Yeo, H. K. Yap, W. Xi, Z. Wang, C.-H. Yeow, and C. T. Lim, "Flexible and stretchable strain sensing actuator for wearable soft robotic applications," *Advanced Materials Technologies*, vol. 1, no. 3, p. 1600018, may 2016.

[13] H. Yousef, M. Boukallel, and K. Althoefer, "Tactile sensing for dexterous in-hand manipulation in roboticsa review," *Sensors and Actuators A: Physical*, vol. 167, no. 2, pp. 171 – 187, 2011, solid-State Sensors, Actuators and Microsystems Workshop.

[14] L. Viry, A. Levi, M. Totaro, A. Mondini, V. Mattoli, B. Mazzolai, and L. Beccai, "Flexible three-axial force sensor for soft and highly sensitive artificial touch," *Advanced Materials*, vol. 26, no. 17, pp. 2659–2664, feb 2014.

[15] B. Nie, R. Li, J. Cao, J. D. Brandt, and T. Pan, "Flexible transparent iontronic film for interfacial capacitive pressure sensing," *Advanced Materials*, vol. 27, no. 39, pp. 6055–6062, sep 2015.

[16] C. Majidi, "Soft robotics: A perspective—current trends and prospects for the future," *Soft Robotics*, vol. 1, no. 1, pp. 5–11, mar 2014.

[17] G. P. Agrawal, *Fiber-optic communication systems*, 3rd ed. Wiley, 2010.

[18] A. Yariv and P. Yeh, *Photonics: optical electronics in modern communications*, 6th ed. Oxford University Press, 2007.